Supplementary Note 1.

Reaction scheme used to calculate reacted isoprene and steady-state OH radical concentrations

Evaluation of secondary OH chemistry of 1st generation products from OH + isoprene

		rate coefficient (cm^3 $molecule^{-1}$ s^{-1})	
O_3 + TME	$\rightarrow$ $0.92 \times OH$ + $0.08 \times HO_2$ + products	1.0×10^{-15} [1]	(1)
OH + TME	$\rightarrow$ products	1.0×10^{-10} [2]	(2)
O_3 + isoprene	$\rightarrow$ $0.26 \times OH$ + $0.26 \times HO_2$ + products	1.3×10^{-17} [1]	(3)
HO_2 + HO_2	$\rightarrow$ H_2O_2 + O_2	1.6×10^{-12} [5]	(4)
O_3 + HO_2	$\rightarrow$ OH + 2 O_2	2.0×10^{-15} [5]	(5)
OH + isoprene	$\rightarrow$ $y \times$ prod1 + products	1.0×10^{-10} [2]	(6)
OH + prod1	$\rightarrow$ prod2	1.0×10^{-10}	(7)

Needed OH and HO_2 radical yields from ozonolysis reactions are taken from literature.[2-4] In the case of O_3 + TME, a HO_2 yield of 0.08 is assumed formed via a pathway other than CI decomposition that results in an OH radical yield of 0.92.

Modelling reveals that under the chosen conditions of the experiment, [TME] = 2.0×10^{11} and [isoprene] = 2.5×10^{12} molecules cm^{-3} and the reaction time 7.9 s, the assumed "prod1" produces only 0.00034 - 0.026% of secondary products via pathway (7) for the range of ozone concentrations of 1.2 - 95×10^{10} molecules cm^{-3} independent of the formation yield "y".
For example, assuming y = 1 in pathway (6) (that stands roughly for HO-$C_5H_8O_2$ production), 1.67×10^7 of "prod1" and 56 molecules cm^{-3} of "prod2" are formed for the lowest ozone concentration. In the case of the highest ozone concentration, 1.32×10^9 of "prod1" and 3.49×10^5 molecules cm^{-3} of "prod2" are produced.
Thus, secondary OH chemistry cannot significantly convert 1st generation products on the one hand, and cannot significantly form 2nd generation products on the other hand.

Supplementary Note 2.

Reaction scheme based on Teng et al.[6] incl. rate coefficients at T = 297 K

Pathways (1) - (5) are identical with those as given in Supplementary Note 1. Equation 6 has been modified according to the nascent RO_2 distribution given by Teng et al.[6]

		rate coefficient (cm^3 $molecule^{-1}$ s^{-1} or s^{-1})	
O_3 + TME	$\rightarrow$ 0.92 × OH + 0.08 × HO_2 + products	1.0×10^{-15} [1]	(1)
OH + TME	$\rightarrow$ products	1.0×10^{-10} [2]	(2)
O_3 + isoprene	$\rightarrow$ 0.26 × OH + 0.26 × HO_2 + products	1.3×10^{-17} [1]	(3)
HO_2 + HO_2	$\rightarrow$ H_2O_2 + O_2	1.6×10^{-12} [5]	(4)
O_3 + HO_2	$\rightarrow$ OH + 2 O_2	2.0×10^{-15} [5]	(5)
OH + isoprene	$\rightarrow$ 0.315 × *trans* OH-adduct I + 0.315 × *cis* OH-adduct I + 0.111 × *trans* OH-adduct II + 0.259 × *cis* OH-adduct II	1.0×10^{-10} [70]	(6a)
trans OH-adduct I + O_2	$\rightarrow$ *E*-δ-HO-RO_2 I	3.2×10^{-13}	(8)
E-δ-HO-RO_2 I	$\rightarrow$ *trans* OH-adduct I + O_2	16	(9)
trans OH-adduct I + O_2	$\rightarrow$ β-HO-RO_2 I	7.8×10^{-13}	(10)
β-HO-RO_2 I	$\rightarrow$ *trans* OH-adduct I + O_2	1.6	(11)
cis OH-adduct I + O_2	$\rightarrow$ β-HO-RO_2 I	7.8×10^{-13}	(12)
β-HO-RO_2 I	$\rightarrow$ *cis* OH-adduct I + O_2	0.29	(13)
cis OH-adduct I + O_2	$\rightarrow$ *Z*-δ-HO-RO_2 I	1.2×10^{-13}	(14)
Z-δ-HO-RO_2 I	$\rightarrow$ *cis* OH-adduct I + O_2	22	(15)

Z-δ-HO-RO_2 I	→ 1,6 H-shift	0.36	(16)
β-HO-RO_2 I	→ 1,5 H-shift	0.0	(17)
trans OH-adduct II + O_2	→ *E*-δ-HO-RO_2 II	4.9×10^{-13}	(18)
E-δ-HO-RO_2 II	→ *trans* OH-adduct II + O_2	3.7	(19)
trans OH-adduct II + O_2	→ β-HO-RO_2 II	7.1×10^{-13}	(20)
β-HO-RO_2 II	→ *trans* OH-adduct II + O_2	0.3	(21)
cis OH-adduct II + O_2	→ β-HO-RO_2 II	7.1×10^{-13}	(22)
β-HO-RO_2 II	→ *cis* OH-adduct II + O_2	0.14	(23)
cis OH-adduct I + O_2	→ *Z*-δ-HO-RO_2 I	2.1×10^{-13}	(24)
Z-δ-HO-RO_2 II	→ *cis* OH-adduct II + O_2	10	(25)
Z-δ-HO-RO_2 II	→ 1,6 H-shift	3.7	(26)
β-HO-RO_2 II	→ 1,5 H-shift	0.0	(27)
E-δ-HO-RO_2 I + HO_2	→ HO-C_5H_8OOH + O_2	1.74×10^{-13} [8]	(28)
β-HO-RO_2 I + HO_2	→ HO-C_5H_8OOH + O_2	1.74×10^{-13} [8]	(29)
Z-δ-HO-RO_2 I + HO_2	→ HO-C_5H_8OOH + O_2	1.74×10^{-13} [8]	(30)
E-δ-HO-RO_2 II + HO_2	→ HO-C_5H_8OOH + O_2	1.74×10^{-13} [8]	(31)
β-HO-RO_2 II + HO_2	→ HO-C_5H_8OOH + O_2	1.74×10^{-13} [8]	(32)
Z-δ-HO-RO_2 II + HO_2	→ HO-C_5H_8OOH + O_2	1.74×10^{-13} [8]	(33)

Supplementary Note 3.

Reaction scheme based on Peeters et al.[7] incl. rate coefficients at T = 298 K

Pathways (1) - (5) are identical with those as given in Supplementary Note 1. Equation 6 has been modified according to the nascent RO_2 distribution given by Peeters et al.[7]

		rate coefficient (cm^3 $molecule^{-1}$ s^{-1} or s^{-1})	
O_3 + TME	→ 0.92 × OH + 0.08 × HO_2 + products	1.0×10^{-15} [1]	(1)
OH + TME	→ products	1.0×10^{-10} [2]	(2)
O_3 + isoprene	→ 0.26 × OH + 0.26 × HO_2 + products	1.3×10^{-17} [1]	(3)
HO_2 + HO_2	→ H_2O_2 + O_2	1.6×10^{-12} [5]	(4)
O_3 + HO_2	→ OH + 2 O_2	2.0×10^{-15} [5]	(5)
OH + isoprene	→ 0.31 × *trans* OH-adduct I + 0.31 × *cis* OH-adduct I + 0.093 × *trans* OH-adduct II + 0.217 × *cis* OH-adduct II	1.0×10^{-10} [2]	(6b)
trans OH-adduct I + O_2	→ *E*-δ-HO-RO_2 I	1.0×10^{-13}	(8)
E-δ-HO-RO_2 I	→ *trans* OH-adduct I + O_2	4.0	(9)
trans OH-adduct I + O_2	→ β-HO-RO_2 I	6.0×10^{-13}	(10)
β-HO-RO_2 I	→ *trans* OH-adduct I + O_2	0.38	(11)
cis OH-adduct I + O_2	→ β-HO-RO_2 I	6.0×10^{-13}	(12)
β-HO-RO_2 I	→ *cis* OH-adduct I + O_2	0.054	(13)
cis OH-adduct I + O_2	→ *Z*-δ-HO-RO_2 I	7.0×10^{-13}	(14)
Z-δ-HO-RO_2 I	→ *cis* OH-adduct I + O_2	4.8	(15)

Z-δ-HO-RO_2 I	→ 1,6 H-shift	0.52	(16)
β-HO-RO_2 I	→ 1,5 H-shift	0.00065	(17)
trans OH-adduct II + O_2	→ *E*-δ-HO-RO_2 II	1.0×10^{-13}	(18)
E-δ-HO-RO_2 II	→ *trans* OH-adduct II + O_2	0.12	(19)
trans OH-adduct II + O_2	→ β-HO-RO_2 II	7.0×10^{-13}	(20)
β-HO-RO_2 II	→ *trans* OH-adduct II + O_2	0.026	(21)
cis OH-adduct II + O_2	→ β-HO-RO_2 II	7.0×10^{-13}	(22)
β-HO-RO_2 II	→ *cis* OH-adduct II + O_2	0.018	(23)
cis OH-adduct I + O_2	→ *Z*-δ-HO-RO_2 I	4.0×10^{-13}	(24)
Z-δ-HO-RO_2 II	→ *cis* OH-adduct II + O_2	0.7	(25)
Z-δ-HO-RO_2 II	→ 1,6 H-shift	5.7	(26)
β-HO-RO_2 II	→ 1,5 H-shift	0.0012	(27)
E-δ-HO-RO_2 I + HO_2	→ HO-C_5H_8OOH + O_2	1.74×10^{-13} [8]	(28)
β-HO-RO_2 I + HO_2	→ HO-C_5H_8OOH + O_2	1.74×10^{-13} [8]	(29)
Z-δ-HO-RO_2 I + HO_2	→ HO-C_5H_8OOH + O_2	1.74×10^{-13} [8]	(30)
E-δ-HO-RO_2 II + HO_2	→ HO-C_5H_8OOH + O_2	1.74×10^{-13} [8]	(31)
β-HO-RO_2 II + HO_2	→ HO-C_5H_8OOH + O_2	1.74×10^{-13} [8]	(32)
Z-δ-HO-RO_2 II + HO_2	→ HO-C_5H_8OOH + O_2	1.74×10^{-13} [8]	(33)

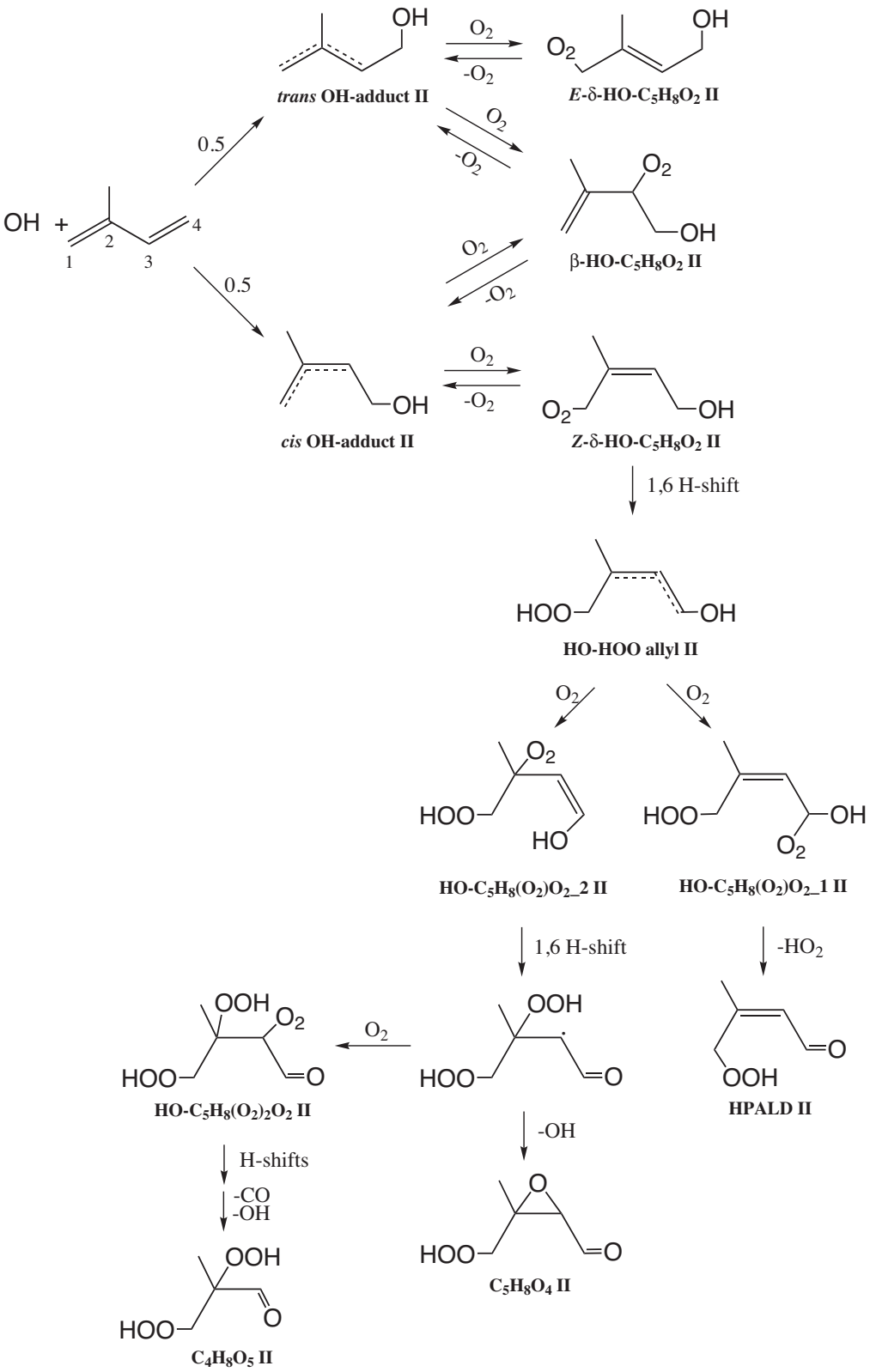

Supplementary Figure 1. First reaction steps starting from OH attack at the 4-position. Possible bimolecular RO_2 radical reactions are not shown. Corresponding reaction scheme for the OH attack at the 1-position is given in Figure 1 in the main body.

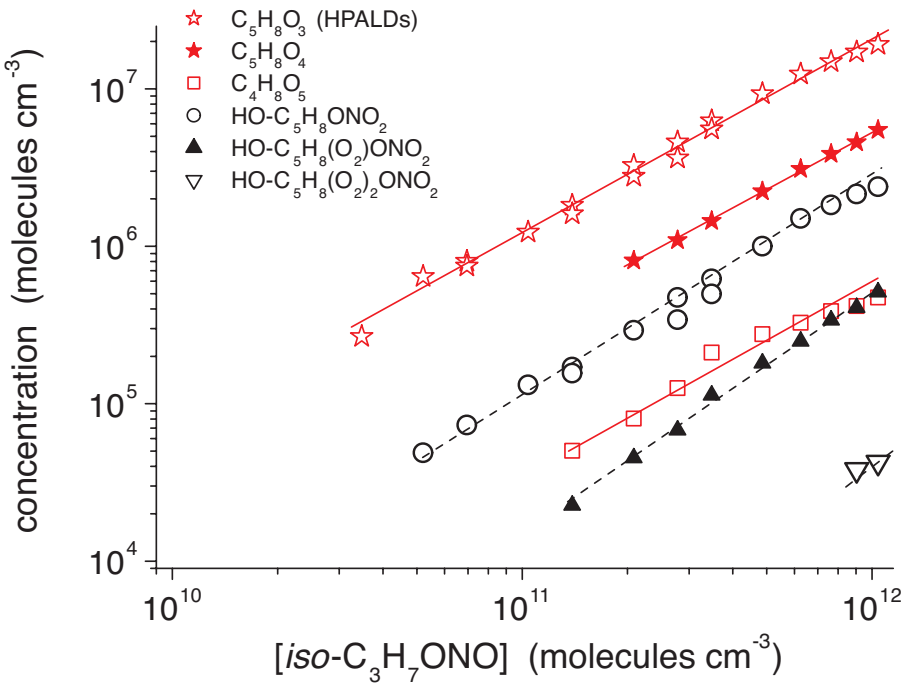

Supplementary Figure 2. Isopropyl nitrite photolysis as OH radical source.
OH radical formation increases with rising *iso*-C_3H_7ONO concentration for constant photolysis conditions and constant [isoprene] = 5.0×10^{11} molecules cm^{-3}, reaction time of 7.9 s. Ethyl-aminium served as the reagent ion. Results for the RO_2 radicals are not shown. Given concentrations represent lower limits.

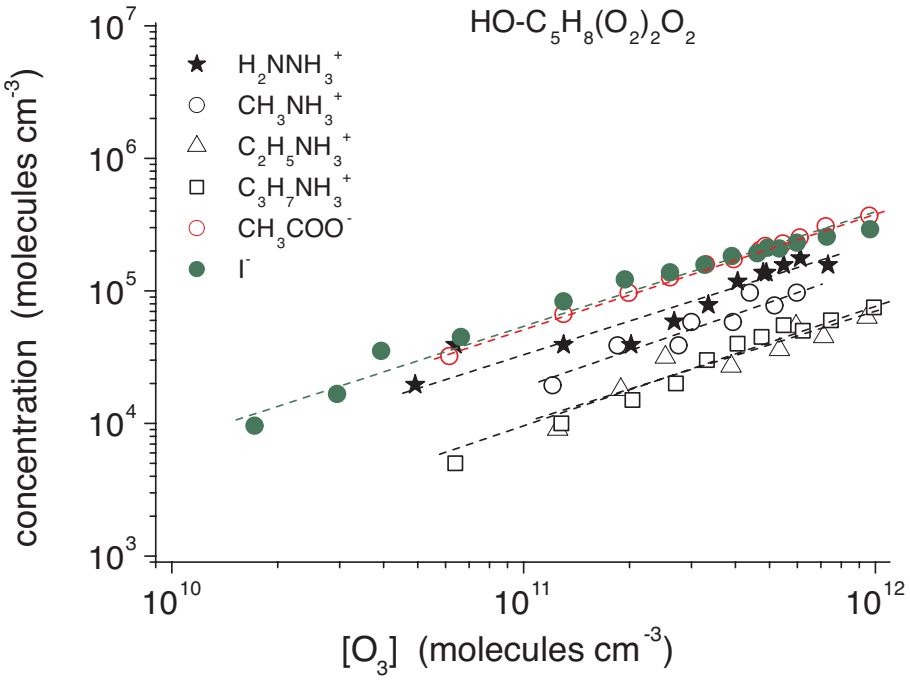

Supplementary Figure 3. Lower limit HO-$C_5H_8(O_2)_2O_2$ concentrations using different reagent ions. Reactant concentrations are [O_3] = (1.2 - 95) × 10^{10}, [TME] = 2.0×10^{11} and [isoprene] = 2.5×10^{12} molecules cm^{-3} and the reaction time 7.9 s. Obtained signals were only slightly above the background level in the case of the measurements using the aminiums or hydrazinium for ionization. It is to be noted, that generally the background level in the positive mode was clearly higher than in the negative mode

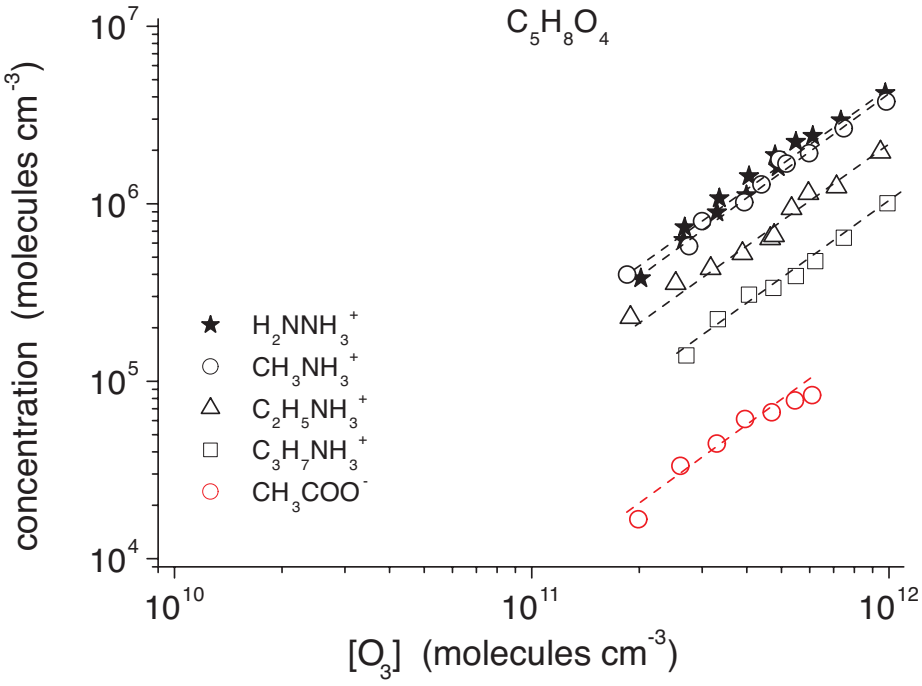

Supplementary Figure 4. Lower limit $C_5H_8O_4$ concentrations using different reagent ions. Reactant concentrations are $[O_3] = (1.2 - 95) \times 10^{10}$, [TME] = 2.0×10^{11} and [isoprene] = 2.5×10^{12} molecules cm^{-3} and the reaction time 7.9 s. Measurements based on iodide ionization were affected by signal interference from other products.

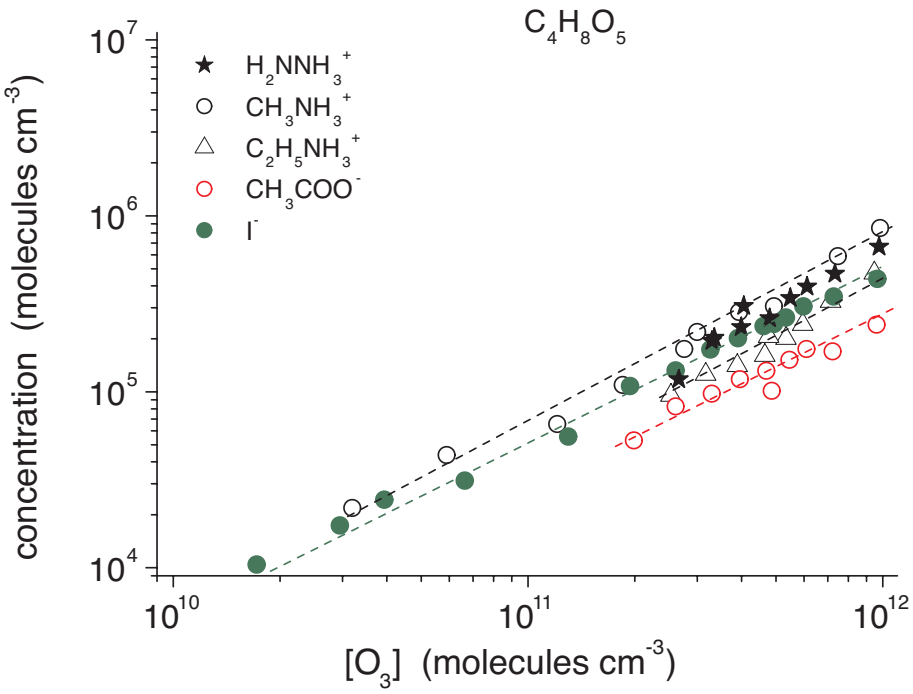

Supplementary Figure 5. Lower limit $C_4H_8O_5$ concentrations using different reagent ions. Reactant concentrations are $[O_3] = (1.2 - 95) \times 10^{10}$, [TME] = 2.0×10^{11} and [isoprene] = 2.5×10^{12} molecules cm^{-3} and the reaction time 7.9 s. Measurements by means of n-propyl-aminium failed because of a very high background signal in the range of the corresponding cluster mass. Note, $C_4H_8O_5$ concentrations resulting from hydrazinium ionization have been obtained applying a peak fitting procedure because of the strong influence of other substances appearing at 169.121 and 169.165 Th, very close to the $(C_4H_8O_5)H_2NNH_3^+$ cluster at 169.082 Th.

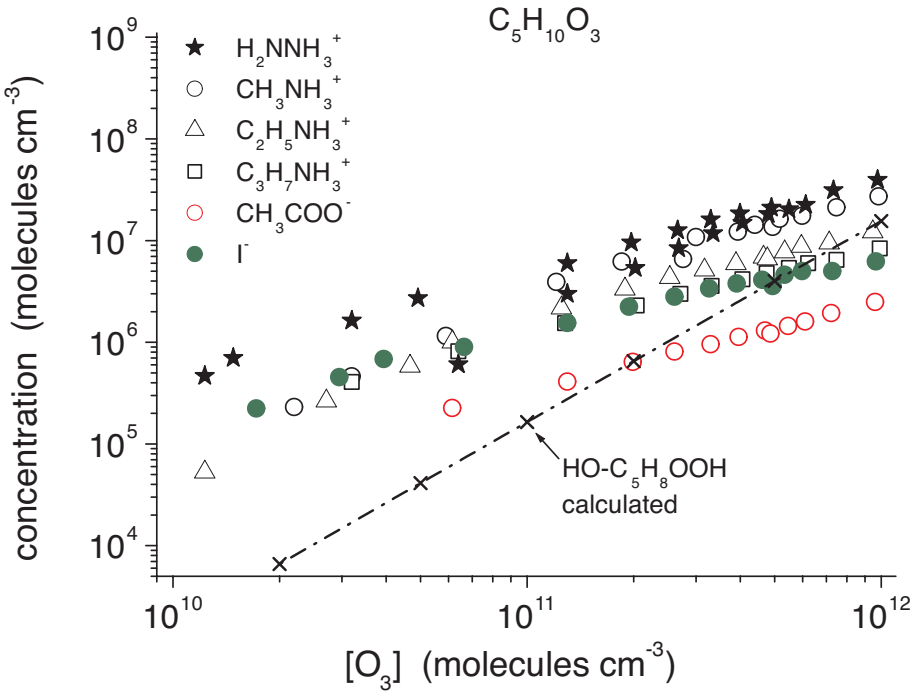

Supplementary Figure 6. Lower limit $C_5H_{10}O_3$ concentrations using different reagent ions. Reactant concentrations are $[O_3] = (1.2 - 95) \times 10^{10}$, [TME] = 2.0×10^{11} and [isoprene] = 2.5×10^{12} molecules cm^{-3} and the reaction time 7.9 s. Modelling of the hydroxy hydroperoxide concentrations, $HO\text{-}C_5H_8OOH$, has been done based on the reaction mechanism given by Teng et al.[6], see Supplementary Note 2.

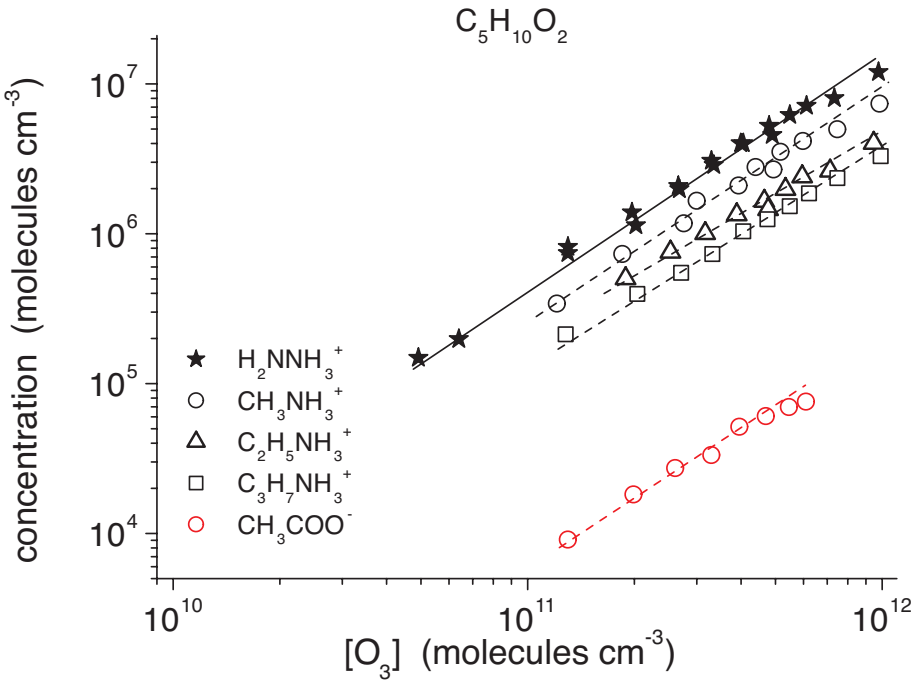

Supplementary Figure 7. Lower limit $C_5H_{10}O_2$ concentrations using different reagent ions. Reactant concentrations are $[O_3] = (1.2 - 95) \times 10^{10}$, [TME] = 2.0×10^{11} and [isoprene] = 2.5×10^{12} molecules cm^{-3} and the reaction time 7.9 s. Measurements using iodide as the reagent ion failed due to a very high background signal.

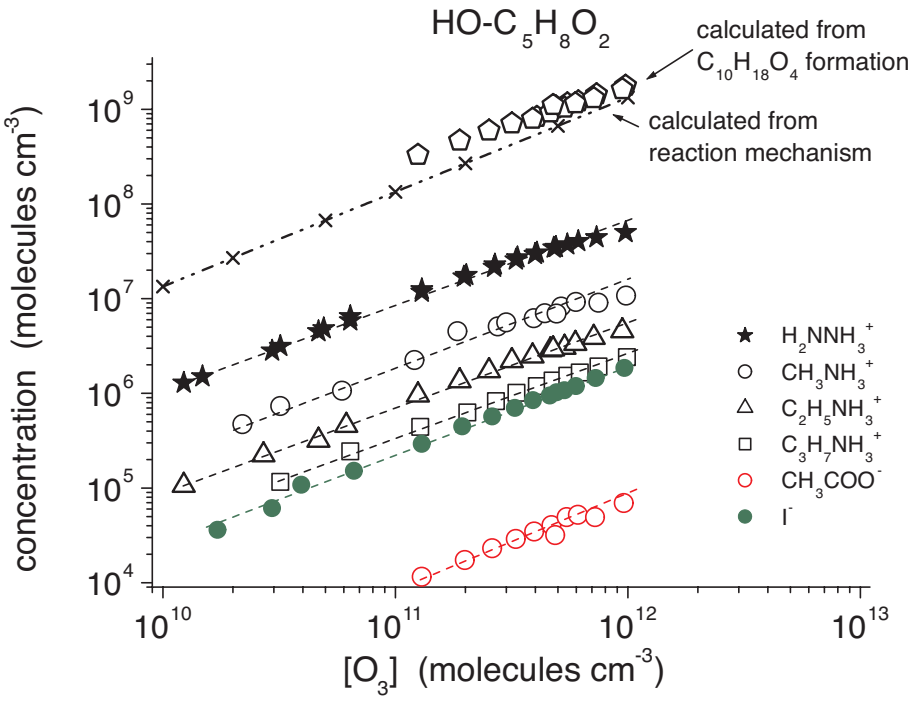

Supplementary Figure 8. Lower limit $HO\text{-}C_5H_8O_2$ concentrations and comparison with calculations. Supplementary Figure 8 is identical with Figure 4a from the main body showing additionally the calculated $HO\text{-}C_5H_8O_2$ radical concentrations derived from the measured $C_{10}H_{18}O_4$ accretion product concentrations, $HO\text{-}C_5H_8O_2 + HO\text{-}C_5H_8O_2 \rightarrow C_{10}H_{18}O_4 + O_2$, according to $[HO\text{-}C_5H_8O_2]_t = (3\ [C_{10}H_{18}O_4]_t / t / k_3)^{0.5}$. The relationship between the concentrations of accretion products and the corresponding RO_2 radicals for our reaction conditions is explained in ref.9. The calculated $HO\text{-}C_5H_8O_2$ concentrations, "calculated from reaction mechanism", have been obtained based on the mechanism given by Teng et al.[6] including the $HO\text{-}C_5H_8O_2 + HO_2$ reaction, see Supplementary Note 2.

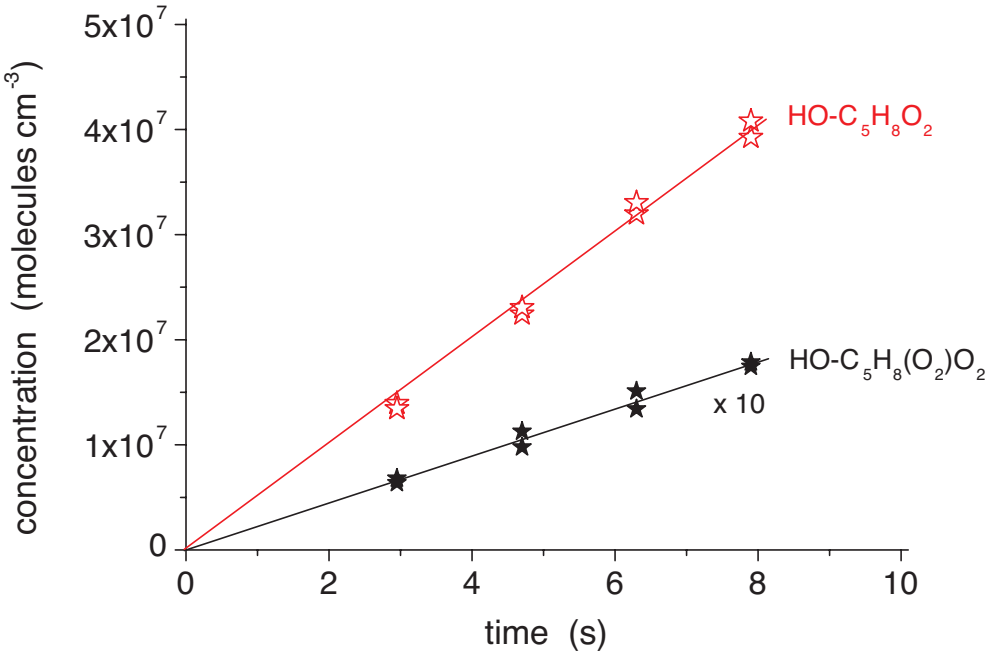

Supplementary Figure 9. Time dependent measurement of HO-$C_5H_8(O_2)_\alpha O_2$ with $\alpha = 0$ and 1. Analysis was carried out using hydrazinium ionization. Reactant concentrations are $[O_3] = 1.04 \times 10^{12}$, [TME] = 2.0×10^{11} and [isoprene] = 2.5×10^{12} molecules cm^{-3}.

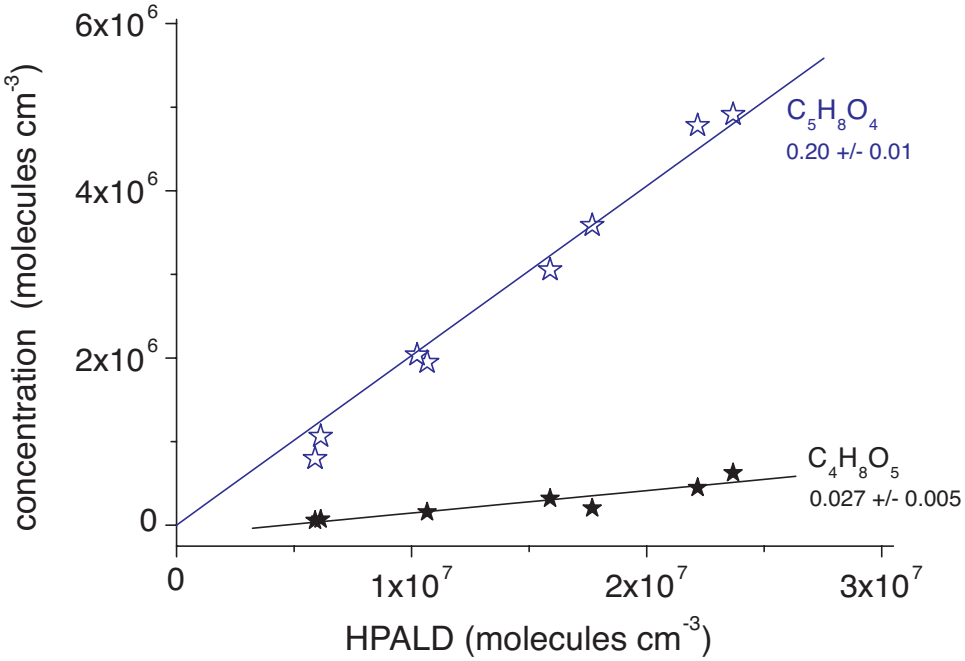

Supplementary Figure 10. Concentrations of $C_5H_8O_4$ and $C_4H_8O_5$ relative to HPALD. Data were taken from experiments given in Figure 7 from the main text.

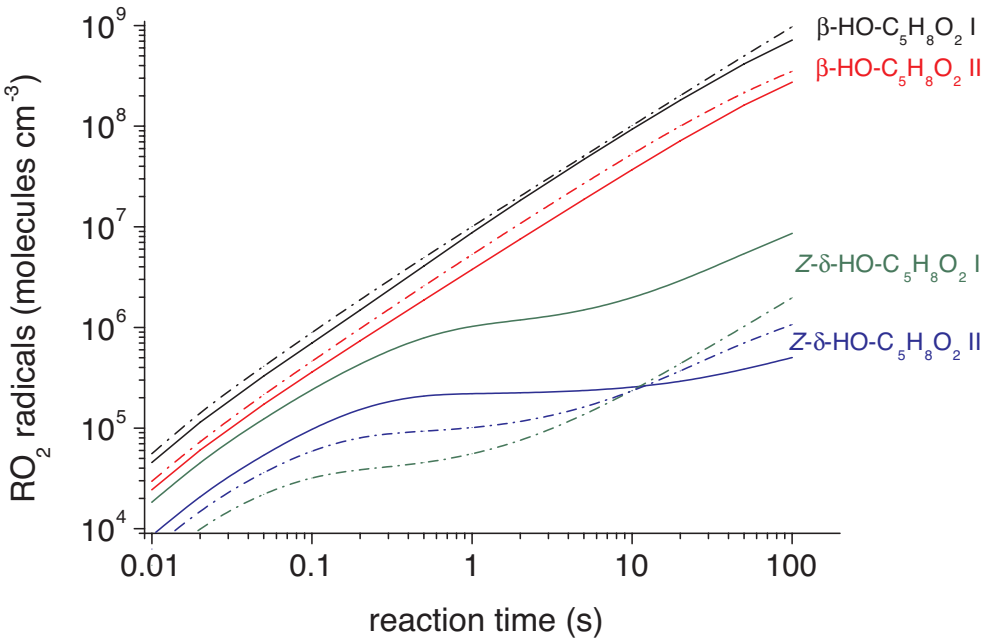

Supplementary Figure 11. Calculated RO_2 radical concentrations using literature data. Calculations have been done based on Peeters et al.[7], full lines, or Teng et al.[6], dashed-dotted lines. Reaction schemes are given in Supplementary Note 3 and Supplementary Note 2, respectively. Reactant concentrations are $[O_3] = 1.0 \times 10^{11}$, [TME] = 2.0×10^{11} and [isoprene] = 2.5×10^{12} molecules cm^{-3}.

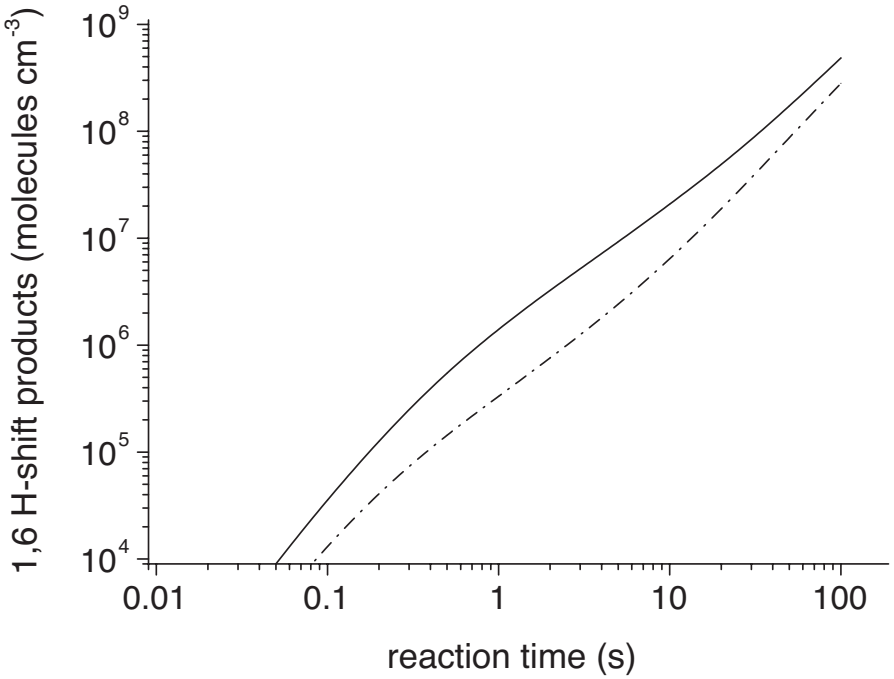

Supplementary Figure 12. Calculated total 1,6 H-shift product concentrations using literature data. Calculations have been done based on Peeters et al.[7], full line, or Teng et al.[6], dashed-dotted line. Reaction schemes are given in Supplementary Note 3 and Supplementary Note 2, respectively. Reactant concentrations are $[O_3] = 1.0 \times 10^{11}$, [TME] = 2.0×10^{11} and [isoprene] = 2.5×10^{12} molecules cm^{-3}.

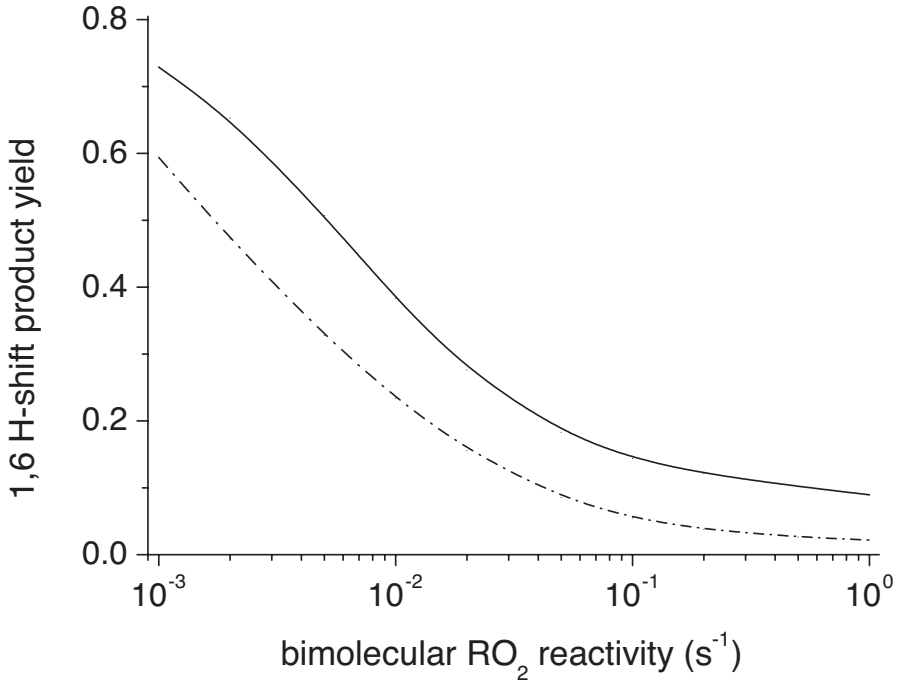

Supplementary Figure 13. 1,6 H-shift product yields as a function of bimolecular RO_2 reactivity. Constant reactant concentrations of 2×10^6 for OH and 5×10^{10} molecules cm^{-3} for isoprene have been considered and a reaction time of 5 h. Calculations have been done based on Peeters et al.[7], full line, or Teng et al.[6], dashed-dotted line. Reaction schemes are given in Supplementary Note 3 and Supplementary Note 2, respectively.

Supplementary Table 1. Formation enthalpies ΔH of ion-molecule clusters.

The formation enthalpies ΔH of the ion-molecule clusters in kcal/mol have been calculated at the DLPNO-CCSD(T)/def2-QZVPP//ωB97X-D/aug-cc-pVTZ level of theory at 298 K. Product structures are given in Figure 1 of the main body.

	Z-δ-HO-$C_5H_8O_2$ I	**β-HO-$C_5H_8O_2$ I**	**HO-$C_5H_8(O_2)O_2$_1 I**	**HPALD I**	**$C_4H_8O_5$ I**
$H_2NNH_3^+$	-30.7	-27.5	-28.8	-33.3	-36.2
$CH_3NH_3^+$	-27.3	-25.3	-26.7	-30.6	-32.6
$C_3H_7NH_3^+$	-25.3	-24.2	-24.4	-28.5	-30.4
CH_3COO^-	-25.8	-27.9	-39.1	-31.9	-40.5
I^-	-17.2	-18.1	-23.9	-20.9	-26.7

Supplementary Table 2. Formation free energies ΔG of ion-molecule clusters.

The formation free energies ΔG of the ion-molecule clusters in kcal/mol have been calculated at the DLPNO-CCSD(T)/def2-QZVPP//ωB97X-D/aug-cc-pVTZ level of theory at 298 K. Product structures are given in Figure 1 of the main body.

	Z-δ-HO-$C_5H_8O_2$ I	**β-HO-$C_5H_8O_2$ I**	**HO-$C_5H_8(O_2)O_2$_1 I**	**HPALD I**	**$C_4H_8O_5$ I**
$H_2NNH_3^+$	-20.4	-17.3	-19.7	-22.0	-26.2
$CH_3NH_3^+$	-17.2	-15.1	-19.2	-19.2	-23.0
$C_3H_7NH_3^+$	-15.7	-14.0	-14.9	-17.2	-21.0
CH_3COO^-	-16.1	-16.8	-28.9	-20.5	-30.2
I^-	-12.5	-11.0	-18.5	-13.4	-20.6

Supplementary Table 3. Comparison of calculated and measured cluster masses.

Comparison of calculated exact cluster masses with measured cluster masses obtained from measurements using hydrazinium for ionization.

Product	Exact mass (Th) (product)$H_2NNH_3^+$	Measured mass (Th) (product)$H_2NNH_3^+$	Disturbing signals
$C_5H_8O_3$	149.092	149.092	
$C_5H_8O_4$	165.087	165.112	
$C_4H_8O_5$	169.082	169.077	169.121, 169.165
HO-$C_5H_8O_2$	150.099	150.099	
HO-$C_5H_8(O_2)O_2$	182.089	182.083	
HO-$C_5H_8(O_2)_2O_2$	214.079	214.076	
$C_{10}H_{18}O_4$	235.165	235.136	
$C_{10}H_{18}O_6$	267.155	267.141	
$C_5H_{10}O_2$	135.113	135.112	
$C_5H_{10}O_3$	151.108	151.112	

Supplementary references

1. Witter, M., Berndt, T., Böge, O., Stratmann, F. & Heintzenberg, J. Gas-phase ozonolysis: Rate coefficients for a series of terpenes and rate coefficients and OH yields for 2-methyl-2-butene and 2,3-dimethyl-2-butene. *Int. J. Chem. Kinet.* **34**, 394-403 (2002).
2. Calvert, J. G., Atkinson, R., Kerr, J. A. Madronich, S., Moortgat, G. K., Wallington, T. J. & Yarwood, G. The mechanism of atmospheric oxidation of the alkenes. (Oxford University Press, 2000).
3. Berndt, T. & Böge, O. Formation of phenol and carbonyls from the atmospheric reaction of OH radicals with benzene. *Phys. Chem. Chem. Phys.* **8**, 1205-1214 (2006).
4. Malkin, T. L., Goddard, A., Heard, D. E. & Seakins, P. W. Measurements of OH and HO_2 yields from the gas phase ozonolysis of isoprene. *Atmos. Chem. Phys.* **10**, 1441-1459 (2010).
5. Atkinson, R., Baulch, D. L., Cox, R. A., Crowley, J. N., Hampson, R. F. Hynes, R. G. Jenkin, M. E., Rossi, M. J. & Troe, J. Evaluated kinetic and photochemical data for atmospheric chemistry: Volume I – gas phase reactions of O_x, HO_x, NO_x and SO_x species. *Atmos. Chem. Phys.* **4**, 1461-1738 (2004).
6. Teng, A. P., Crounse, J. D. & Wennberg, P. O. Isoprene peroxy radical dynamics. *J. Am. Chem. Soc.* **139**, 5367-5377 (2017).
7. Peeters, J., Müller, J.-F., Stavrakou, T. & Nguyen, T. L. Hydroxyl radical recycling in isoprene oxidation driven by hydrogen bonding and hydrogen tunneling: The upgraded LIM1 mechanism. *J. Phys. Chem. A* **118**, 8625-8643 (2014).
8. Boyd, A. A., Flaud, P.-M., Daugey, N. & Lesclaux, R. Rate constants for RO_2 + HO_2 reactions measured under a large excess of HO_2. *J. Phys. Chem. A* **107**, 818-821 (2003).
9. Berndt, T., Scholz, W., Mentler, B., Fischer, L., Herrmann, H., Kulmala, M. & Hansel, A. Accretion product formation from self- and cross-reactions of RO_2 radicals in the atmosphere. *Angew. Chem. Int. Ed.* **57**, 3820-3824 (2018).